

Efficient Adaptive Activation Rounding for Post-Training Quantization

Zhengyi Li^{1,2} Cong Guo^{1,2} Zhanda Zhu¹ Yangjie Zhou¹ Yuxian Qiu^{1,2} Xiaotian Gao³ Jingwen Leng^{1,2}
Minyi Guo^{1,2}

Abstract

Post-training quantization (PTQ) attracts increasing attention due to its convenience in deploying quantized neural networks. Rounding is the primary source of quantization error, for which previous works adopt the rounding-to-nearest scheme with a constant border of 0.5. This work demonstrates that optimizing rounding schemes can improve model accuracy. By replacing the constant border with a simple border function, we can obtain the minimal error for multiplying two numbers and eliminate the bias of its expected value, which further benefits model accuracy. Based on this insight, we approximate the border function to make the incurred overhead negligible. We also jointly optimize propagated errors and global errors. We finally propose our AQuant framework, which can learn the border function automatically. Extensive experiments show that AQuant achieves noticeable improvements compared with state-of-the-art works and pushes the accuracy of ResNet-18 up to 60.31% under the 2-bit weight and activation post-training quantization.

1. Introduction

Despite the excellent accuracy performance of deep neural networks (DNNs), they have significant memory usage and computing costs. DNN quantization can reduce both computational and storage overhead by converting floating-point numbers into low-bit representations. It has become an effective technique for deploying DNNs on resource-limited devices. The quantization of DNNs can be classified into two categories. Quantization-aware training (QAT) (Esser et al., 2019; Zhuang et al., 2021; Wang et al., 2019; Gong et al., 2019; Shen et al., 2021) trains quantized models from scratch on the entire training dataset. Therefore, QAT is costly and time-consuming. Post-training quantization (Wang et al., 2020; Hubara et al., 2021; Banner et al., 2019b; Guo et al., 2021; Choi et al., 2021; Liu et al., 2021; Shomron et al., 2021; Nagel et al., 2020; Li et al., 2020) (PTQ) has recently attracted increasing interests due to its convenience and ease of deployment. It only requires a

limited dataset (usually 1000 samples) to finetune a trained model.

Rounding is the primary source of quantization error in PTQ. Traditional quantization methods take the nearest rounding for weights, minimizing the mean squared error (MSE) between quantized and full-precision weights. AdaRound (Nagel et al., 2020) shows that a better solution is to learn the rounding scheme by using the MSE of each layer’s output activation as the optimization objective. As for the activation quantization, previous relevant works focus on optimizing its step size. While the activation quantization still adopts the traditional rounding-to-nearest scheme. The underlying assumption for DNN quantization is that errors of each entry (denoted as **element-wise error**) of the dot product cancel out each other so that the output error is trivial. However, the nearest rounding of activations only minimizes MSE of themselves. For varying activations, when multiplied with weights, the element-wise error is not minimized and cannot always cancel out properly, which may lead to the unexpected output error.

In this work, we show that an optimized activation rounding scheme benefits the final model accuracy. The activation quantization is performed at the inference stage, so an both effective and efficient way is needed. To deal with these two challenges, we first show that using a border function to replace the original constant border can produce minimal and unbiased element-wise errors, which further reduces the output error. Based on this insight, we give an approximated solution by parameterizing the border function to make the runtime overhead negligible. We further improve the border function to make it aware of the propagated error of previous layers and the channel-wise error. Finally, equipped with the border function, we establish a PTQ framework AQuant that optimizes the proposed border function. Extensive experiments on popular CNN models and the Transformer model (Vaswani et al., 2017) show that our method significantly outperforms the recent state-of-the-art PTQ baselines (Nagel et al., 2020; Li et al., 2020; Wei et al., 2022) with negligible extra parameters and computation overhead.

The contributions of this work are as follows:

1. We show the benefits of adjusting rounding schemes of activations both experimentally and theoretically, providing a new perspective for the PTQ.
2. We find a linear border function can produce minimal and unbiased element-wise errors. Then, we give an efficient approximation to the border function so that we can exploit it to adjust the rounding schemes at runtime. We further include the impact of the propagated error and the channel-wise error into the border function for better performance.
3. We finally propose a PTQ framework to learn the proposed border function. Extensive experiments on various CNN models and the transformer model show that our method greatly outperforms state-of-the-art PTQ methods under all the precision settings.

2. Preliminaries

Notations The constant or scalar are denoted by italic letters, such as x_i and s . For layer ℓ , we denote $\mathbf{W}^{(\ell)}$ and $\mathbf{w}^{(\ell)}$ as the weight tensor and its flattened version, respectively. Its input tensor is denoted by $\mathbf{X}^{(\ell)}$, and $\mathbf{x}^{(\ell)}$ represents one column of it. We denote $\mathbf{x}'^{(\ell)}$ as the noised version of $\mathbf{x}^{(\ell)}$ caused by the quantization error of previous layers. The activation function (ReLU) and the bias are omitted for simplicity. We denote $\mathbb{E}[\cdot]$ as the expectation operator of \mathbf{x} on the dataset, and the network loss function is represented by $\mathcal{L}(\cdot)$.

For the convolutional layer, we denote the output channel, input channel, and kernel size as o_c , i_c , and k , respectively. The height and width of the input feature map are h_i and w_i , and h_o and w_o are the height and width of the output. In order to unify the feedforward of the convolution layer and the fully connected layer (FC) using matrix multiplication $\mathbf{X}^{(\ell+1)} = \mathbf{W}^{(\ell)} \mathbf{X}^{(\ell)}$ in the following discussion, we explicitly convert the convolution filter from (o_c, i_c, k, k) to $(o_c, i_c \times k \times k)$. The input of convolutional layer is arranged from (i_c, h_i, w_i) to $(i_c \times k \times k, h_o \times w_o)$ using the `img2col` transformation (Paszke et al., 2019). The $h_o \times w_o$ is the number of sliding blocks, and each one has $i_c \times k \times k$ elements in it.

Quantization The uniform quantization and dequantization for the scalar x can be described as $\hat{x} = s \cdot \text{clip}([x - B], \min, \max)$, where s denotes the quantization step size, $\text{clip}(\cdot)$ is the clipping function. $\lceil x - B \rceil$ is the rounding operation. B is the rounding border, which we generalize its definition in Definition 2.1.

Definition 2.1 (Rounding border). Given the error function $g(\Delta x)$, B is called as rounding border iff

- the square of the error function of rounding down

equals the one of rounding up, i.e. $g(-B)^2 = g(1 - B)^2$. The $-B$ and $1 - B$ are errors of rounding up and rounding down, respectively;

- any x with fractional part smaller than B should be rounded down and vice versa.

Especially, the traditional rounding-to-nearest operator is when $g(\Delta x)$ is an identity function and B is the constant 0.5.

Post training quantization Early PTQ methods take the rounding-to-nearest scheme to the model weights, which minimizes the mean square error (MSE) between quantized weight $\hat{\mathbf{W}}$ and original weight \mathbf{W} . A recent study, AdaRound (Nagel et al., 2020), finds that the minimization of weights' MSE is not equivalent to the minimization in final task loss $\mathbb{E}[\mathcal{L}(\hat{\mathbf{w}}, \mathbf{x})]$. They treat the quantization error as a small perturbation to the weight and apply Taylor expansion to the task loss, and obtain

$$\begin{aligned} & \arg \min_{\Delta \mathbf{w}^{(\ell)}} \mathbb{E}[\mathcal{L}(\hat{\mathbf{w}}, \mathbf{x}) - \mathcal{L}(\mathbf{w}, \mathbf{x})] \\ & \stackrel{(a)}{\approx} \arg \min_{\Delta \mathbf{w}_{k,:}^{(\ell)}} \left[\left(\Delta \mathbf{W}_{k,:}^{(\ell)} \mathbf{x}^{(\ell-1)} \right)^2 \right], \end{aligned} \quad (1)$$

where (a) are assumptions made by AdaRound to simplify the problems. Equation (1) decomposes the optimization of the task loss into independent sub-problems. Each sub-problem deals with a single $\mathbf{W}_{k,:}$ and their rounding schemes $\Delta \mathbf{w}^{(\ell)}$ should minimize the expected VDP error. Then they optimize the rounding schemes layer-wisely (or block-wisely (Li et al., 2020; Wei et al., 2022)) based on Equation (1).

3. Method

3.1. Introducing Activation Quantization into the Optimization Objective

The basic operation of DNNs is vector dot product (**VDP**) between activations and weights. The VDP error is the sum of element-wise errors of all additive components, where **element-wise error** is the error of the product of the corresponding entries of quantized activations and weights. Small and unbiased element-wise errors are critical to a trivial VDP error. Here, ‘unbiased’ means the expected element-wise errors are zero, so they can cancel out each other better. The activation quantization requires two steps. It first scales the floating-point values using the step size and then takes rounding to get integer values. Prior works about the activation quantization, including LSQ (Esser et al., 2019), PACT (Choi et al., 2018), and ACIQ (Banner et al., 2019a), focus on the first step by optimizing the step size or the clipping range. But they all assume the nearest

rounding for the second step. Nearest rounding minimizes the MSE of activations themselves but is not aimed at the element-wise error or the VDP error. For various activation vectors, nearest rounding even cannot achieve unbiased rounding error of activations. An extreme example is when the fractional part of all activations is greater than 0.5. Taking the rounding-to-nearest scheme enlarges all activations. Such a mean shift is harmful to accuracy. Finkelstein et al. (2019b) also mentions this problem. Their solution is to finetune the bias of the linear layer, which is still hard to suit varying activations and suffers great accuracy degradation for low-bit quantization. Furthermore, the element-wise error is more unpredictable after multiplying with quantized weights. We later show that the nearest rounding of activations always makes the element-wise errors biased in Section 3.2. Therefore, we hypothesize adaptively adjusting the activation rounding schemes can reduce the VDP errors and improve the accuracy.

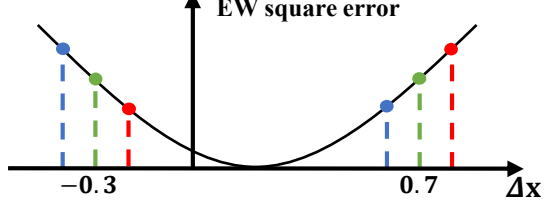
We first extend the previous optimization objective to include the impact of activation quantization. Previous work (Nagel et al., 2020) has shown that a better approach for weight quantization is to use the learned rounding schemes according to Equation (1). However, one deficiency is that the impact of the activation quantization is not explicitly considered in their derivation. One natural extension of the optimization objective should be

$$\arg \min_{\Delta x, \Delta W} \mathbb{E} \left[\left(\left(\mathbf{W}_{i,:}^{(\ell)} + \Delta \mathbf{W}_{i,:}^{(\ell)} \right) \left(\mathbf{x}^{(\ell)} + \Delta \mathbf{x}^{(\ell)} \right) - \mathbf{W}_{i,:}^{(\ell)} \mathbf{x}^{(\ell)} \right)^2 \right] \quad (2a)$$

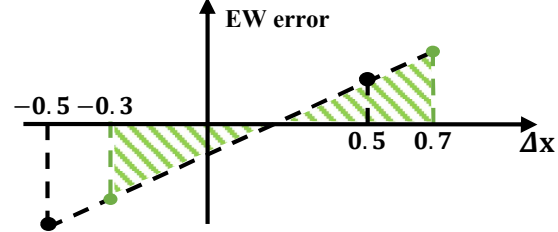
$$= \arg \min_{\Delta x, \Delta W} \mathbb{E} \left[\left(\left(\mathbf{W}_{i,:}^{(\ell)} + \Delta \mathbf{W}_{i,:}^{(\ell)} \right) \Delta \mathbf{x}^{(\ell)} + \Delta \mathbf{W}_{i,:}^{(\ell)} \mathbf{x}^{(\ell)} \right)^2 \right]. \quad (2b)$$

In Equation (2a), the first term defines the dot product between the quantized weight and activation vectors, and the second term is the full-precision dot product. We assume that ΔW is given by the previous methods (Nagel et al., 2020; Li et al., 2020; Wei et al., 2022) and the step size of the activation quantization is given by LSQ (Esser et al., 2019) since they are out of the scope of this work.

Despite the natural generalization, the challenges of adjusting activation rounding are two-fold. First, previous works (Nagel et al., 2020; Li et al., 2020; Wei et al., 2022) learn static rounding schemes for weights. However, due to their dynamicity, similar methods cannot be directly applied to activations. The activation rounding is done at the runtime, and we first need to decide how to adaptively adjust rounding schemes for different activations that can benefit the VDP error. Second, the activation quantization is done at the inference stage. The way we adjust activation rounding must be both computation- and memory-efficient.



(a) The element-wise square error function w.r.t. Δx . Dot lines with the same color represent one rounding pair.



(b) The element-wise error function w.r.t. Δx . Without loss of generality, we assume the $(w + \Delta w)$ is positive. The border $B = 0.3$ results in unbiased element-wise error (green regions).

Figure 1. Illustration of the element-wise error.

3.2. Adaptive Rounding via Border Function

To understand how to adjust activation rounding, our core idea is to use the element-wise error as the guide for activation rounding rather than using the error of the activations themselves. We find that generalizing the constant rounding border 0.5 to a border function can achieve minimal and unbiased element-wise errors, which further reduces the VDP error. Note that we do not claim that our method is the optimal way to minimize objective in Equation (2b), but it is a possible way to optimize it with negligible overhead.

Based on Equation (2b), the element-wise error of the VDP is

$$g(\Delta x) = (w + \Delta w) \Delta x + \Delta w x, \quad (3)$$

where w is one element of vector $\mathbf{W}_{i,:}$ and x is the corresponding activation value. The superscript (ℓ) is omitted for simplicity. We note that the w and x have been scaled by the step size in the following discussion.

Recall the definition of rounding border in Definition 2.1, initially, the error function $g(\Delta x)$ is an identity function that minimizes the square error of x itself, which corresponds to the rounding-to-nearest operator. We replace the error function with the element-wise error in Equation (3). The validity of this substitution comes from an important finding that the definition of the rounding border still holds for element-wise error. We give examples in Figure 1(a) to demonstrate this. Suppose the w , Δw , and x together shape the square curve of $g(\Delta x)$. Note that the curve actually

moves for the different fractional parts of x , but we assume it holds for easy illustration. In this case, the rounding border is 0.3 since the square error is the same for rounding pair $\Delta x^- = -0.3$ and $\Delta x^+ = 0.7$. Any activations with the fractional part smaller than 0.3 should round down (red pair) and vice versa (blue pair). Situations are the same for other combinations of w , Δw , and x .

With the new error function of rounding border, the border becomes a function w.r.t. the activation value. Using Definition 2.1, it satisfies $g(-B^E(x))^2 = g(1 - B^E(x))^2$, from which we can derive

$$B^E(x) = \frac{\Delta w}{w + \Delta w} x + \frac{1}{2}. \quad (4)$$

The superscript E represents the border is computed using only one element of the activation vector. Compared to the constant border $B = 0.5$ in nearest rounding, $\frac{\Delta w x}{w + \Delta w}$ quantitatively defines the effects of the weight and weight error. Details of the derivation can be found in the Appendix.

With the border function, one direct result is the minimal absolute element-wise error. Moreover, the expected element-wise error becomes unbiased. For different inputs, we can assume the fractional part of x uniformly distributes in the interval $[0, 1]$. Then the expected element-wise error w.r.t. different inputs is the integral of Equation (3) from $-B$ to $1 - B$. Following the example in Figure 1(a), the expected value of nearest rounding is negative when taking integral from -0.5 to 0.5 (black region), as illustrated in Figure 1(b). On the contrary, the expected element-wise error is zero using the modified border (green region).

Intuitively, reducing the magnitude of the element-wise error and making it unbiased is beneficial for the VDP error. We give a formal analysis through the central limit theorem (CLT). The CLT states the summation of independent random variables tends toward a normal distribution, despite their original distributions. The expected value and variance of the summation are the sum of the expected value and variance of these random variables, respectively. Previous studies have shown the values in DNNs can be approximated as independent (Kingma et al., 2015). In this way, first, the expected value of the VDP error is also zero, so that it does not incline to accumulate or amplify. Second, the magnitude of the VDP error is also reduced due to the smaller variance of the element-wise error.

Our analysis demonstrates a simple linear border can benefit the error of dot product. The next problem is efficiently obtaining the rounding border at the inference stage. Equation (4) is hard to deploy directly due to the large memory overhead. Take the matrix multiplication of the convolutional layer as an example, each activation value x is multiplied with o_c weight values, where o_c is the number of output channels. Assigning a linear border function for each weight element introduces as many parameters as model

weights and is unacceptable in practice. Moreover, we need to accordingly round x for different weights, which is incompatible with existing DNN computation kernels.

To derive a feasible solution from the previous insight, we let each activation value only be rounded once and its rounding scheme is shared by the o_c weights. In this way, the rounding border considers the overall effects of o_c weights. To achieve this, we parameterize the border function as

$$B^E(x) = b_1 \cdot x + b_0, \quad (5)$$

and learn its parameters on the calibration set. With this trade-off between extra parameter numbers and the performance, AQuant only imports $O(\frac{1}{o_c})$ extra parameters compared with the model weights, and we only need to store one version of quantized x . Except for the very small overhead complexity, the rounding border is generated locally for each activation value. Its computation can be easily fused with other operators, such as `img2col` so that the runtime overhead can be ignored.

3.3. Improve the Border Function

We show the linear border function is a feasible solution to adaptively adjust the activation rounding with almost negligible overhead. This section further introduces another two factors that affect the VDP error and our attempts to include them in the border function. Note that any modification to the border function should be subjected to the runtime overhead.

Propagated error The input of layer ℓ includes the propagated errors caused by previous layers. Prior works (Nagel et al., 2020; Li et al., 2020; Wei et al., 2022) handle it implicitly by end-to-end optimization. While we need to verify whether our border function can capture the impact of the propagated error so we consider it explicitly. To this end, we further include the propagated error in the objective (2b)

$$\arg \min_{\Delta \mathbf{x}, \Delta \mathbf{W}} \mathbb{E} \left[((\mathbf{W}_{i,:} + \Delta \mathbf{W}_{i,:}) (\mathbf{x}' + \Delta \mathbf{x}') - \mathbf{W}_{i,:} \mathbf{x})^2 \right]. \quad (6)$$

Note that we change the input from \mathbf{x} to the noised version \mathbf{x}' , and the $\Delta \mathbf{x}'$ is the quantization error based on the noised input. Following the same way when we derive Equation (4), the rounding border now becomes

$$B^E(x') = \frac{\Delta w}{w + \Delta w} x' + \frac{w}{w + \Delta w} e(x') + \frac{1}{2}, \quad (7)$$

where $e(x) = x' - x$ is the propagated error. The newly introduced term $\frac{w}{w + \Delta w} e(x')$ defines the impact of the propagated error. However, the propagated error $e(x')$ is determined by the quantization of previous layers, which is a complex process and is hard to analyze. Therefore, we

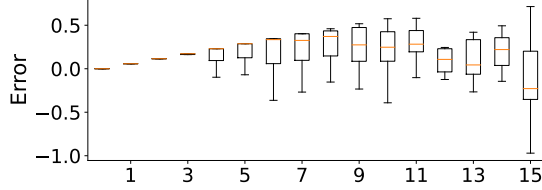


Figure 2. The propagated error w.r.t. the noised activation x' . For ease of understanding, we group x' into 16 clusters according to their magnitude, as listed on the X-axis. Y-axis is the error between noised and full-precision activation.

present an empirical study to handle it through experiments. Our experiments are conducted on ResNet-18 under W2A4 quantization. For a pixel of the input of the second layer, we summarize activation values and their errors on 1024 images. Since the complex process in previous layers produces the errors in a random-like fashion, we only consider fitting the propagated error in the sense of its mean value. As shown in Figure 2, when the magnitude of x' increases, the mean value first slowly deviates from zero and then moves towards zero again. Similar non-linear trends are also observed on other pixels and other layers. In order for the border function to fit this nonlinear relationship, we propose to extend the linear border in the last section to a quadratic border w.r.t. x' , which becomes

$$B^E(x') = b_2 \cdot x'^2 + b_1 \cdot x' + b_0, \quad (8)$$

where b_i are parameters learned through gradient descent on the calibration set. Quadratic function approximately introduces the impact of the propagated error with trivial overhead on top of the linear border.

Border fusion The derived linear (quadratic if considering the propagated error) border is only aware of local information. A border that integrates global information is supposed to be a better solution. As such, we further consider optimizing the border function on a larger scope. To achieve this, we simply take a weighted average for borders to integrate information. Consider the convolutional layer, the activation vector is composed of i_c input channels, with each containing k^2 elements. The intuitive way is to average the border on the whole vector. However, activations and weights from different input channels have varying magnitudes. The gradient descent may only focus on input channels with large scales, which could result in a local minimum. Therefore, we fuse the border within each input channel, which is

$$B^J(\mathbf{x}'_{ik^2:(i+1)k^2}) = \frac{1}{k^2} \sum_{j=ik^2}^{(i+1)k^2-1} B_j^E(x'_j), \quad (9)$$

where $\mathbf{x}'_{ik^2:(i+1)k^2}$ is the i th input channel of vector \mathbf{x}' and B_j^E is the border function of the pixel x'_j . The border

Algorithm 1 Finetune pre-trained model block with rounding border function on one mini-batch

Input: Bit-width M , pre-trained model block composed by layer i to layer j , noised input $\mathbf{X}'^{(i)}$ of layer i and FP output $\mathbf{X}'^{(j+1)}$ of layer j ;

for $\ell = i$ to j **do**

$$\hat{\mathbf{X}}'^{(\ell)} = s^{(\ell)} \cdot \text{clip}([\mathbf{X}'^{(\ell)} - B^{(\ell)}(\mathbf{X}'^{(\ell)})], 0, 2^M - 1);$$

$$\mathbf{X}'^{(\ell+1)} = (\mathbf{W}^{(\ell)} + \Delta \mathbf{W}^{(\ell)}) \hat{\mathbf{X}}'^{(\ell)};$$

end for

Compute MSE between $\mathbf{X}'^{(j+1)}$ and $\mathbf{X}'^{(\ell+1)}$ and do backward propagation;

Output: Border functions, activation step sizes, and weight schemes;

value is averaged and then shared within the input channel. This method may not be the optimal way to integrate global information, but it introduces no additional parameters, and the introduced average operation can still be easily fused with the `img2col` kernel.

3.4. AQuant

Based on the effective and efficient border function, we finally propose AQuant. Substituting the Δx by $[\mathbf{x}' - B(\mathbf{x}')]$ – \mathbf{x}' , the optimization objective in Equation (2b) becomes:

$$\min_{B(\cdot), \Delta \mathbf{W}} \mathbb{E} \left[((\mathbf{W} + \Delta \mathbf{W})([\mathbf{x}' - B(\mathbf{x}')]) - \mathbf{W}\mathbf{x})^2 \right]. \quad (10)$$

The $B(\mathbf{x}')$ here means to apply Equation (9) to each input channel of the activation vector. The optimization of weight rounding schemes follows previous methods (Nagel et al., 2020; Li et al., 2020; Wei et al., 2022) and we only denote as optimizing $\Delta \mathbf{W}$ for simplicity. The step size of activation quantization is learned using LSQ (Esser et al., 2019). We use gradient descent to optimize the above formula for each model block, following Li et al. (2020). Details of finetuning a block with our border function are shown in Algorithm 1. For each block, it takes noisy inputs with all preceding layers quantized. Each layer in the block forwards with quantized activations and weights. Then we compute the MSE loss between quantized output and full-precision output and update weight rounding schemes and border functions. We also design specific techniques to stabilize the optimization process of the border function, which we present more detail in the Appendix.

Overhead analysis We first analyze the extra parameter ratio of the border function using the convolutional layer. For the reshaped convolutional filter with shape $(o_c, i_c \times k^2)$, since we let all output channels share the border function, we need $i_c \times k^2$ border functions. The quadratic function triples the number of parameters and results in $3 \times i_c \times k^2$

Table 1. Accuracy comparison on fully quantized models. All results include LSQ during optimization.

Methods	Bits	Res18	Res50	MNV2	Reg600MF	Reg3.2GF	MNasx2
Baseline	W32A32	71.01	76.62	72.63	73.53	78.45	76.52
AdaRound	W4A4	69.49	74.82	67.53	70.87	76.41	71.80
BRECQ	W4A4	69.45	75.05	68.29	70.96	76.64	73.24
QDrop	W4A4	69.61	75.40	68.57	71.19	76.76	73.54
AQuant	W4A4	70.03	75.58	69.15	71.68	77.03	73.78
AdaRound	W2A4	63.64	66.61	44.90	58.95	64.66	51.03
BRECQ	W2A4	64.84	70.27	53.43	62.41	71.21	62.11
QDrop	W2A4	65.16	70.71	54.22	63.59	71.34	63.78
AQuant	W2A4	66.63	71.11	56.74	65.71	72.98	65.27
AdaRound	W3A3	66.00	69.72	48.92	61.99	68.65	50.48
BRECQ	W3A3	66.01	71.73	54.66	63.79	71.75	64.16
QDrop	W3A3	66.65	72.38	57.68	65.37	72.69	66.43
AQuant	W3A3	67.97	73.20	58.56	67.11	74.09	68.96
BRECQ	W2A2	51.12	51.36	7.44	29.84	41.88	13.32
QDrop	W2A2	54.19	57.38	11.45	41.53	54.61	28.65
AQuant	W2A2	60.31	60.04	14.19	46.61	57.48	30.31

parameters. Compared to the weight tensor with $o_c \times i_c \times k^2$ elements, the extra parameter ratio is $3/o_c$, which is very small due to the hundreds or thousands o_c . A similar analysis can also be applied to the fully connected layer.

Then we analyze the computing overhead. Taking the scalar multiplication as the basic operation, the complexity of the convolutional layer to compute one sample is $O(o_c \times i_c \times k^2 \times h_i \times w_i)$. As for the border function, for a total of $i_c \times k^2 \times h_i \times w_i$ activations, the border function evaluates the quadratic function for each activation, requiring $O(i_c \times k^2 \times h_i \times w_i)$ operations and is only $O(1/o_c)$ compared to the innate computation of the layer. This ratio is also because the o_c weights share one border. Moreover, $B(x)$ only includes element-wise computation and an average operation. Such a computation pattern is more efficient than the dominating operation of DNNs, matrix multiplication, in the sense of computing parallelism and memory access. The computation of the border function can be easily fused with other kernels, such as `img2col`. Even though we assign the border function a higher bitwidth than the backbone model, the overhead is still small enough to ignore. Exact latency is highly dependent on the target hardware and the implementation of the GPU kernel. Therefore, we implement the fused kernel and give experiments in Section 4.3 to show the efficiency.

4. Experiments

To verify the effectiveness of AQuant, we first compare AQuant with other SOTA PTQ approaches. Then we conduct ablation experiments and demonstrate the negligible overhead of AQuant.

Experimental setup Our algorithms are implemented using PyTorch (Paszke et al., 2019) and evaluated on Nvidia GPU V100. The experiments include image classification on ImageNet and natural language processing tasks on the GLUE benchmark. On both of them, we sample 1024 instances as the calibration set. The weight quantization follows AdaRound (Nagel et al., 2020) (QDrop (Wei et al., 2022) on the ImageNet dataset) and adopts per-channel weight quantization. The step size of activation quantization follows Esser et al. (2019). Prior works (Nagel et al., 2019; Bondarenko et al., 2021) optimize the activation step size after the rounding schemes of weights are learned. In our implementation, we optimize the step size of the activation together with the weight rounding schemes for all baselines, which has been proven to achieve great improvements compared to the former optimization pipeline (Wei et al., 2022). More detailed settings are described in the Appendix.

4.1. Comparison with SOTA Methods

ImageNet To evaluate the effectiveness of AQuant, we conduct experiments on 6 CNN models using ImageNet (Deng et al., 2009) dataset, including ResNet-18 & 50 (He et al., 2016), MobileNetV2 (Sandler et al., 2018), MNasNet (Tan et al., 2019) and RegNet (Radosavovic et al., 2020). The models we use cover common designs of CNNs, including the residue connection, depthwise-separable convolution, and group convolution. We optimize the border function using Adam optimizer (Kingma & Ba, 2014) with learning rate 1e-3. For lightweight models MobileNetV2 and MNasNet, we degrade the quadratic border to a linear border to reduce the extra parameter ratio. We choose baselines from two aspects, optimization on rounding schemes and activation quantization optimization. For works re-

Table 2. W4A4 quantization results on GELU benchmark (except WNLI). All cases include LSQ during optimization. \dagger Reports F1 score for MRPC and QQP. \ddagger Reports Pearson correlation for STS-B. ψ Reports matched accuracy for MNLI.

Method	CoLA	SST-2	MRPC \dagger	STS-B \ddagger	QQP \dagger	MNLI ψ	QNLI	RTE
FP baseline	58.59	91.28	89.54	89.14	87.98	84.06	91.19	70.39
AdaRound	43.82	82.45	87.92	83.13	74.24	65.77	83.29	55.60
AQuant	45.23	84.06	88.62	83.87	75.87	68.57	83.45	61.37

lated to rounding schemes, we compare AQuant with three strong baselines AdaRound (Nagel et al., 2020), BRECQ (Li et al., 2020), and QDrop (Wei et al., 2022). AdaRound and BRECQ optimize the weight rounding schemes layer-wisely and block-wisely. QDrop randomly drops the quantization of activations when optimizing rounding schemes of weights. For works about the activation quantization, as far as we know, previous works only optimize the step size and we pick LSQ as the used method. We do not list it separately but use it by default in all experiments since merely using it suffers great accuracy loss. We report results of baselines using the open-source codes of QDrop (Wei et al., 2022)¹ with unified settings.

We present the results of fully-quantized models in Table 1. We focus on quantization lower than 8-bit as W8A8 is almost loss-free in previous works. Our method outperforms previous PTQ methods in all cases. The benefits of AQuant become more prominent as the bitwidth decreases. For challenging models like MobileNetV2 and MNasNet, we also achieve significant improvements compared with other methods. We find that ResNet-18 and ResNet-50 achieve more than 60% accuracy in the extremely low W2A2 quantization. It is worth noting that AQuant only has around 1% accuracy loss for 4-bit quantization on many models.

GLUE benchmark Although our method is discussed mainly on the convolutional layer, it can be applied to the fully connected layer of the transformer model. We use the fine-tuned BERT model and the GLUE benchmark from Huggingface (Wolf et al., 2020). Our implementation is based on the open-sourced code of Bondarenko et al. (2021)², which implements AdaRound. All the intermediate activations are quantized except the embedding and the classification layers. Other settings are kept the same. Since all the linear layers of the BERT is the fully connected layer, we do not use border fusion mentioned in Section 3.3. We adopt W4A6 to quantize the transformer model. AQuant surpasses the baseline in all the tasks. Our method improves the accuracy by close to two percent, even when the results are already close to full-precision accuracy.

¹<https://github.com/wimh966/QDrop>

²<https://github.com/qualcomm-ai-research/transformer-quantization>

Table 3. Ablation experiments of border function and fusion.

Methods	Strategy	Bits	Res18	Reg600M
		Linear	W2A2	59.14
Border function	Quadratic	W2A2	60.31	46.61
	Linear	W3A3	67.59	66.78
	Quadratic	W3A3	67.97	67.11
	No fusion	W2A2	58.56	44.95
Border fusion	Fusion	W2A2	60.31	46.61
	No fusion	W3A3	67.76	66.93
	Fusion	W3A3	67.97	67.11

4.2. Ablation Study

Border function We verify the effectiveness of the quadratic border function in reducing the propagated error. We compare it with the linear border function. Other settings are kept the same as in the previous section. In Table 3, the quadratic border outperforms the linear border on both models and bitwidths.

Border fusion We then test the effectiveness of border fusion on error cancellation. “Fusion” is exact the AQuant mentioned in Section 3.4 and “No fusion” only uses the element-wise border function. According to Table 3, border fusion further improves the accuracy by error cancellation. On extremely low bitwidth, fusion produces more apparent improvements.

We find that the gap of both border function and border fusion shrink for 3-bit quantization because the effects of propagated errors and rounding errors get small. This also gives the freedom to use the linear border function or the element-wise function for high-bit quantization to save more overhead.

4.3. Overhead Analysis

Ratio of AQuant parameters AQuant introduces only $1/o_c$ extra number of parameters. Existing works have shown that 8-bit quantization can achieve almost lossless accuracy (Jacob et al., 2018). In practice, the border function can be post-quantized to 16 bits to guarantee precision. For ResNet-18 and ResNet-50, ratios of the extra number of parameters are 0.81% and 0.64%, respectively. If weights

utilize 4-bit quantization, AQuant only increases 3% of the model size. For RegNet-600MF and RegNet-3200MF, the ratios of the extra number of parameters are 2.82% and 2.14%, and the extra model size is around 10%. For small models MobileNetV2 and MNasNet, we degrade the border function as linear and ratios of the extra number of parameters are 4.56% and 8.27%. As for the transformer model, the output channel is at least 768. The extra model size is only 0.75%. The ratio of extra model size can be further reduced by training quantized border functions, such as 8-bit quantization.

Runtime overhead As analyzed in the previous section, AQuant introduces only $1/o_c$ extra computation complexity at the inference stage. Our profiling experiments show that the overhead is even more negligible due to the benefits of kernel fusion. We adopt element-wise border function $B(x)$ since its improvement is enough in most cases. The convolution includes two operators, `img2col` and `matmul`. Due to the simple computation pattern, we fuse the computation of $B(x)$ with the `img2col` operator, which saves the overhead of launching kernel and memory swapping. Our implementation is based on the open-source code of Caffe (Jia et al., 2014) and is tested on Nvidia V100. Other DNN frameworks or hardware should present similar results. Using batch size 32, we list the execution times of each layer of ResNet-18. As shown in Figure 3, executing times of fused convolution is close to the original times. On the whole model, the extra latency is 0.0028ms, which is only 5.11% of the original inference time. Note that we only implement a naive fused kernel, and a tuned implementation can perform better.

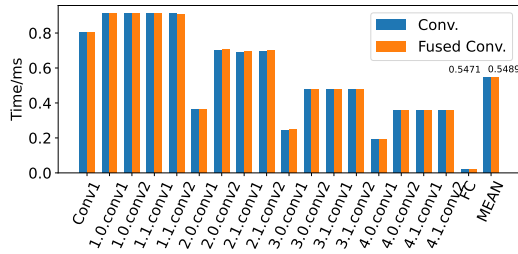


Figure 3. Latency breakdown on the ResNet-18. The experiment is executed 100 times and uses the average value.

5. Related Work

The quantization of deep neural networks can be classified into two categories. Quantization-aware Training (QAT) trains a quantized model on the full training dataset from scratch while Post-training quantization (PTQ) only requires a limited dataset (usually 1k images) to finetune a pre-trained model. Despite the promising accuracy reached

by QAT (Esser et al., 2019; Wang et al., 2019; Gong et al., 2019; Shen et al., 2021), it suffers from the training costs and cumbersome hyper-parameter search. On the contrary, PTQ has been attracting a lot of interest due to its convenience. Studies include optimizing the clipping range of the weight (Choukroun et al., 2019; Banner et al., 2019b). Zhao et al. (2019) split channels to exclude outlier values, achieving lower bit quantization on the cost of extra computation. Other works include mix precision (Cai et al., 2020), synthetic data for PTQ (Zhang et al., 2021), and data-free quantization (Guo et al., 2021).

The most relevant track is optimizing the rounding schemes of weights. AdaRound (Nagel et al., 2020) first theoretically proves that the nearest rounding, which minimizes the MSE of weight itself, is not optimal. Instead, they propose to learn the rounding scheme that minimizes the MSE of the layer output. BRECQ (Li et al., 2020) further proposes to reconstruct the weight block-wisely. However, these works and other works still apply the nearest rounding to activations, and their methods cannot be directly applied to the activation rounding due to its dynamicity. Existing works tend to overlook activation rounding due to the challenge of handling its dynamicity and runtime overhead. They optimize the activation quantization from other aspects. Some works (Banner et al., 2019a; Choi et al., 2018; Esser et al., 2019) optimize the step size to minimize the MSE of activations themselves. Others (Finkelstein et al., 2019a; Nagel et al., 2019) compensate for the mean activation shift by correcting the bias of the linear layer. QDrop (Wei et al., 2022) also highlights the importance of activation error and uses weights to absorb its impact. But they all assume the rounding-to-nearest at the rounding stage, which we show produces non-minimal and biased element-wise errors. In this work, we adaptively round the activations via a lightweight border function, which is a new perspective for the PTQ.

6. Conclusion

This paper introduces AQuant, which makes up for the blank of activation rounding in PTQ algorithms. We first theoretically demonstrate minimal and unbiased element-wise errors can be achieved by using a linear border function. Based on this insight, we parameterize the function to efficiently round activations at runtime. We also improve the function by jointly optimizing the propagated error and considering the channel-wise error. Extensive experiments validate the efficiency of AQuant. It achieves higher accuracy on all kinds of bitwidths and significantly improves the low bitwidth, with negligible extra parameters and computation overhead. Future works include exploiting the insight to design a more effective border function and achieve smaller runtime overhead by algorithm and hardware co-design.

References

Banner, R., Nahshan, Y., Hoffer, E., and Soudry, D. ACIQ: Analytical clipping for integer quantization of neural networks, 2019a. URL <https://openreview.net/forum?id=B1x33sC9KQ>.

Banner, R., Nahshan, Y., and Soudry, D. Post training 4-bit quantization of convolutional networks for rapid-deployment. *Advances in Neural Information Processing Systems*, 32, 2019b.

Bondarenko, Y., Nagel, M., and Blankevoort, T. Understanding and overcoming the challenges of efficient transformer quantization. In *Proceedings of the 2021 Conference on Empirical Methods in Natural Language Processing*, pp. 7947–7969, Online and Punta Cana, Dominican Republic, November 2021. Association for Computational Linguistics. doi: 10.18653/v1/2021.emnlp-main.627. URL <https://aclanthology.org/2021.emnlp-main.627>.

Cai, Y., Yao, Z., Dong, Z., Gholami, A., Mahoney, M. W., and Keutzer, K. Zeroq: A novel zero shot quantization framework. In *Proceedings of the IEEE/CVF Conference on Computer Vision and Pattern Recognition*, pp. 13169–13178, 2020.

Choi, J., Wang, Z., Venkataramani, S., Chuang, P. I.-J., Srinivasan, V., and Gopalakrishnan, K. Pact: Parameterized clipping activation for quantized neural networks. *arXiv preprint arXiv:1805.06085*, 2018.

Choi, K., Hong, D., Park, N., Kim, Y., and Lee, J. Qimera: Data-free quantization with synthetic boundary supporting samples. In Ranzato, M., Beygelzimer, A., Dauphin, Y., Liang, P., and Vaughan, J. W. (eds.), *Advances in Neural Information Processing Systems*, volume 34, pp. 14835–14847. Curran Associates, Inc., 2021. URL <https://proceedings.neurips.cc/paper/2021/file/7cc234202e98d2722580858573fd0817-Paper.pdf>.

Choukroun, Y., Kravchik, E., Yang, F., and Kisilev, P. Low-bit quantization of neural networks for efficient inference. In *2019 IEEE/CVF International Conference on Computer Vision Workshop (ICCVW)*, pp. 3009–3018. IEEE, 2019.

Deng, J., Dong, W., Socher, R., Li, L.-J., Li, K., and Fei-Fei, L. Imagenet: A large-scale hierarchical image database. In *2009 IEEE Conference on Computer Vision and Pattern Recognition*, pp. 248–255, 2009. doi: 10.1109/CVPR.2009.5206848.

Esser, S. K., McKinstry, J. L., Bablani, D., Appuswamy, R., and Modha, D. S. Learned step size quantization. In *International Conference on Learning Representations*, 2019.

Finkelstein, A., Almog, U., and Grobman, M. Fighting quantization bias with bias. *CoRR*, abs/1906.03193, 2019a. URL <http://arxiv.org/abs/1906.03193>.

Finkelstein, A., Almog, U., and Grobman, M. Fighting quantization bias with bias. *arXiv preprint arXiv:1906.03193*, 2019b.

Gong, R., Liu, X., Jiang, S., Li, T., Hu, P., Lin, J., Yu, F., and Yan, J. Differentiable soft quantization: Bridging full-precision and low-bit neural networks. In *Proceedings of the IEEE/CVF International Conference on Computer Vision*, pp. 4852–4861, 2019.

Guo, C., Qiu, Y., Leng, J., Gao, X., Zhang, C., Liu, Y., Yang, F., Zhu, Y., and Guo, M. Squant: On-the-fly data-free quantization via diagonal hessian approximation. In *International Conference on Learning Representations*, 2021.

He, K., Zhang, X., Ren, S., and Sun, J. Deep residual learning for image recognition. In *Proceedings of the IEEE conference on computer vision and pattern recognition*, pp. 770–778, 2016.

Hubara, I., Nahshan, Y., Hanani, Y., Banner, R., and Soudry, D. Accurate post training quantization with small calibration sets. In *International Conference on Machine Learning*, pp. 4466–4475. PMLR, 2021.

Jacob, B., Kligys, S., Chen, B., Zhu, M., Tang, M., Howard, A., Adam, H., and Kalenichenko, D. Quantization and training of neural networks for efficient integer-arithmetic-only inference. In *Proceedings of the IEEE conference on computer vision and pattern recognition*, pp. 2704–2713, 2018.

Jia, Y., Shelhamer, E., Donahue, J., Karayev, S., Long, J., Girshick, R., Guadarrama, S., and Darrell, T. Caffe: Convolutional architecture for fast feature embedding. In *Proceedings of the 22nd ACM international conference on Multimedia*, pp. 675–678, 2014.

Kingma, D. P. and Ba, J. Adam: A method for stochastic optimization. *arXiv preprint arXiv:1412.6980*, 2014.

Kingma, D. P., Salimans, T., and Welling, M. Variational dropout and the local reparameterization trick. *Advances in neural information processing systems*, 28, 2015.

Li, Y., Gong, R., Tan, X., Yang, Y., Hu, P., Zhang, Q., Yu, F., Wang, W., and Gu, S. Brecq: Pushing the limit of post-training quantization by block reconstruction. In *International Conference on Learning Representations*, 2020.

Liu, Z., Wang, Y., Han, K., Zhang, W., Ma, S., and Gao, W. Post-training quantization for vision transformer. In Ranzato, M., Beygelzimer, A., Dauphin, Y., Liang, P., and Vaughan, J. W. (eds.), *Advances in Neural Information Processing Systems*, volume 34, pp. 28092–28103. Curran Associates, Inc., 2021. URL <https://proceedings.neurips.cc/paper/2021/file/ec8956637a99787bd197eacd77acce5e-Paper.pdf>.

Nagel, M., Baalen, M. v., Blankevoort, T., and Welling, M. Data-free quantization through weight equalization and bias correction. In *Proceedings of the IEEE/CVF International Conference on Computer Vision*, pp. 1325–1334, 2019.

Nagel, M., Amjad, R. A., Van Baalen, M., Louizos, C., and Blankevoort, T. Up or down? adaptive rounding for post-training quantization. In *International Conference on Machine Learning*, pp. 7197–7206. PMLR, 2020.

Paszke, A., Gross, S., Massa, F., Lerer, A., Bradbury, J., Chanan, G., Killeen, T., Lin, Z., Gimelshein, N., Antiga, L., et al. Pytorch: An imperative style, high-performance deep learning library. *Advances in neural information processing systems*, 32, 2019.

Radosavovic, I., Kosaraju, R. P., Girshick, R., He, K., and Dollár, P. Designing network design spaces. In *Proceedings of the IEEE/CVF Conference on Computer Vision and Pattern Recognition*, pp. 10428–10436, 2020.

Sandler, M., Howard, A., Zhu, M., Zhmoginov, A., and Chen, L.-C. Mobilenetv2: Inverted residuals and linear bottlenecks. In *Proceedings of the IEEE conference on computer vision and pattern recognition*, pp. 4510–4520, 2018.

Shen, M., Liang, F., Gong, R., Li, Y., Li, C., Lin, C., Yu, F., Yan, J., and Ouyang, W. Once quantization-aware training: High performance extremely low-bit architecture search. In *Proceedings of the IEEE/CVF International Conference on Computer Vision*, pp. 5340–5349, 2021.

Shomron, G., Gabbay, F., Kurzum, S., and Weiser, U. Post-training sparsity-aware quantization. In Ranzato, M., Beygelzimer, A., Dauphin, Y., Liang, P., and Vaughan, J. W. (eds.), *Advances in Neural Information Processing Systems*, volume 34, pp. 17737–17748. Curran Associates, Inc., 2021. URL <https://proceedings.neurips.cc/paper/2021/file/9431c87f273e507e6040fcb07dcb4509-Paper.pdf>.

Tan, M., Chen, B., Pang, R., Vasudevan, V., Sandler, M., Howard, A., and Le, Q. V. Mnasnet: Platform-aware neural architecture search for mobile. In *Proceedings of the IEEE/CVF Conference on Computer Vision and Pattern Recognition*, pp. 2820–2828, 2019.

Vaswani, A., Shazeer, N., Parmar, N., Uszkoreit, J., Jones, L., Gomez, A. N., Kaiser, Ł., and Polosukhin, I. Attention is all you need. *Advances in neural information processing systems*, 30, 2017.

Wang, P., Chen, Q., He, X., and Cheng, J. Towards accurate post-training network quantization via bit-split and stitching. In *International Conference on Machine Learning*, pp. 9847–9856. PMLR, 2020.

Wang, Z., Lu, J., Tao, C., Zhou, J., and Tian, Q. Learning channel-wise interactions for binary convolutional neural networks. In *Proceedings of the IEEE/CVF Conference on Computer Vision and Pattern Recognition*, pp. 568–577, 2019.

Wei, X., Gong, R., Li, Y., Liu, X., and Yu, F. QDrop: Randomly dropping quantization for extremely low-bit post-training quantization. In *International Conference on Learning Representations*, 2022. URL <https://openreview.net/forum?id=ySQH0oDyp7>.

Wolf, T., Debut, L., Sanh, V., Chaumond, J., Delangue, C., Moi, A., Cistac, P., Rault, T., Louf, R., Funtowicz, M., Davison, J., Shleifer, S., von Platen, P., Ma, C., Jernite, Y., Plu, J., Xu, C., Scao, T. L., Gugger, S., Drame, M., Lhoest, Q., and Rush, A. M. Transformers: State-of-the-art natural language processing. In *Proceedings of the 2020 Conference on Empirical Methods in Natural Language Processing: System Demonstrations*, pp. 38–45, Online, October 2020. Association for Computational Linguistics. URL <https://www.aclweb.org/anthology/2020.emnlp-demos.6>.

Zhang, X., Qin, H., Ding, Y., Gong, R., Yan, Q., Tao, R., Li, Y., Yu, F., and Liu, X. Diversifying sample generation for accurate data-free quantization. In *Proceedings of the IEEE/CVF Conference on Computer Vision and Pattern Recognition*, pp. 15658–15667, 2021.

Zhao, R., Hu, Y., Dotzel, J., De Sa, C., and Zhang, Z. Improving neural network quantization without retraining using outlier channel splitting. In *International conference on machine learning*, pp. 7543–7552. PMLR, 2019.

Zhuang, B., Tan, M., Liu, J., Liu, L., Reid, I., and Shen, C. Effective training of convolutional neural networks with low-bitwidth weights and activations. *IEEE Transactions on Pattern Analysis and Machine Intelligence*, 2021.